Research Article | Vol. 25, No. 15 | 24 Jul 2017 | OPTICS EXPRESS 18152
Optics EXPRESS

Simultaneous multi-segmented mirror orientation test system using a digital aperture based on sheared Fourier analysis

HEEJOO CHOI,[1] ISAAC TRUMPER,[1] MATTHEW DUBIN,[1] WENCHUAN ZHAO,[1,2] AND DAE WOOK KIM[1,3,*]

[1]*College of Optical Sciences, University of Arizona, 1630 E. University Blvd., Tucson, AZ 85721, USA*
[2]*Chinese Academy of Sciences, The Institute of Optics and Electronics, Chengdu 610209, China*
[3]*Steward Observatory, University of Arizona, 933 N. Cherry Ave., Tucson, AZ 85719, USA*
**letter2dwk@hotmail.com*

Abstract: This paper presents a simultaneous multi-segmented mirror orientation test system (SMOTS) using localized sheared images. A CMOS camera captures images of reflected 2D sinusoidal patterns from the test mirrors as their orientation changes. Surface orientation is measured to within 0.8 μrad (0.16 arcseconds) for a flat mirror. In addition, we measure the variation of seven mirror segments simultaneously. Furthermore, SMOTS is applied to measure the orientation of two concave mirrors with an accuracy of 2.7 μrad (0.56 arcseconds). The measurement time for seven segments is 0.07 s. This technique can monitor the mirror segment orientation in an open/closed-loop for various optical setups.

OCIS codes: (220.1140) Alignment; (120.3930) Metrological instrumentation; (120.5700) Reflection; (350.1260) Astronomical optics.

References and links

1. J. M. Oschmann, M. Clampin, and H. MacEwen, "Special Section Guest Editorial: Space Telescopes," Opt. Eng. **52**(9), 091801 (2013).
2. J. S. Fender, "Future trends in large space optics," Proc. SPIE **4013**, 682–686 (2000).
3. M. Johns, P. McCarthy, K. Raybould, A. Bouchez, A. Farahani, J. Filgueira, G. Jacoby, S. Shectman, and M. Sheehan, "Giant Magellan Telescope: overview," Proc. SPIE **8444**, 84441H (2012).
4. R. Gilmozzi and J. Spyromilio, "The 42m European ELT: status," Proc. SPIE **7012**, 701219 (2008).
5. N. Yaitskova and K. Dohlen, "Tip-tilt error for extremely large segmented telescopes: detailed theoretical point-spread-function analysis and numerical simulation results," J. Opt. Soc. Am. A **19**(7), 1274–1285 (2002).
6. G. Chanan, M. Troy, F. Dekens, S. Michaels, J. Nelson, T. Mast, and D. Kirkman, "Phasing the mirror segments of the Keck telescopes: the broadband phasing algorithm," Appl. Opt. **37**(1), 140–155 (1998).
7. J. M. Rodriguez-Ramos and J. J. Fuensalida, "Local Piston Detection of a Segmented Mirror Telescope with Curvature Sensing of Wavefronts Affected by Atmospheric Turbulence. Numerical Simulations," NATO ASI Ser., Ser. C **501**, 355–358 (1997).
8. J. M. Rodriguez-Ramos and J. J. Fuensalida, "Piston detection of a segmented mirror telescope using a curvature sensor: preliminary results with numerical simulations," Proc. SPIE **2871**, 613–616 (1997).
9. N. Yaitskova, K. Dohlen, P. Dierickx, and L. Montoya, "Mach-Zehnder interferometer for piston and tip-tilt sensing in segmented telescopes: theory and analytical treatment," J. Opt. Soc. Am. A **22**(6), 1093–1105 (2005).
10. X. Dai, O. Sasaki, J. E. Greivenkamp, and T. Suzuki, "High accuracy, wide range, rotation angle measurement by the use of two parallel interference patterns," Appl. Opt. **36**(25), 6190–6195 (1997).
11. J. Yuan and X. Long, "CCD-area-based autocollimator for precision small-angle measurement," Rev. Sci. Instrum. **74**(3), 1362–1365 (2003).
12. P. Su, R. E. Parks, L. Wang, R. P. Angel, and J. H. Burge, "Software configurable optical test system: a computerized reverse Hartmann test," Appl. Opt. **49**(23), 4404–4412 (2010).
13. Y. Wu, Y. Cao, Z. Huang, M. Lu, and D. Chen, "Improved composite Fourier transform profilometry," Opt. Laser Technol. **44**(7), 2037–2042 (2012).
14. W. H. Southwell, "Wave-front estimation from wave-front slope measurements," J. Opt. Soc. Am. **70**(8), 998–1006 (1980).
15. I. Trumper, H. Choi, and D. W. Kim, "Instantaneous phase shifting deflectometry," Opt. Express **24**(24), 27993–28007 (2016).
16. L. Li, W. Zhao, F. Wu, and Y. Liu, "Flat mirror tilt and piston measurement based on structured light reflection," Opt. Express **22**(22), 27707–27716 (2014).

#296595 https://doi.org/10.1364/OE.25.018152
Journal © 2017 Received 23 May 2017; revised 6 Jul 2017; accepted 11 Jul 2017; published 19 Jul 2017

Optics EXPRESS

17. B. C. Platt and R. Shack, "History and Principles of Shack-Hartmann Wavefront Sensing," J. Refract. Surg. **17**(5), S573–S577 (2001).
18. J. D. Gaskill, *Linear Systems, Fourier Transforms, and Optics* (John Wiley and Sons, 1978), Chap. 7.

1. Introduction

To see deeper into our Universe, scientists need to build larger telescopes [1,2]. The use of a multi-segment primary mirror is very useful to achieve this for large aperture telescopes, and has fabrication advantages [3,4]. However, this type of telescope can suffer from specific problems associated with segment misalignment. High accuracy fine alignment of the segmented mirror is essential to achieve optimum performance. It is also important to note that maintenance of the mirror segments (or any other multi-component optical systems) will necessitate realignment.

There are various symptoms of misalignment in the segments, which include degradation in image quality. A point spread function (PSF) is a well-known metric to judge the image quality, and it can be an indicator for alignment [5]. This mathematical approach needs an influence parameter for each segment. However, this method does not have a one-to-one correspondence between image quality and segment orientation. This ambiguity increases with the number of segments. Therefore, a more straightforward and simple method of detecting misalignment in the mirror segments is desirable.

To directly measure each segment, the Shack-Hartmann test [6] and curvature sensor [7,8] have been adapted for alignment. The Shack-Hartmann test is sensitive in a tip-tilt measurement, but it measures wavefront slopes (not surface slopes) at a certain conjugate plane and it is insensitive to local piston errors. The curvature sensor is convenient for a piston alignment test. An interferometric approach can also be adopted for segmented alignment [9]. Interferometry provides an abundance of high accuracy information about the orientation of each mirror, but is limited by its small dynamic range, and a stable environment is required to make a measurement.

For the normal application of an angular measurement, laser interferometers [10], and photoelectric autocollimators [11] are standard solutions. Their accuracy is state of the art, but they have limited capability when measuring multiple segments and surface shapes.

The capabilities of deflectometry that have been developed for measuring the shape of a specular surface [12] can be applied to alignment. The concept of deflectometry is based on the reverse Hartmann test, which measures optical slope by calculating the deflected angle of rays individually (pixel-by-pixel in detector approach). To get the slope data from deflectometry, many calculations are essential, such as phase unwrapping [12], Fourier transforms, filtering and inverse transforms [13], and slope integration [14]. Some advanced versions include instantaneous measurement technology [15] and structured light deflectometry systems. Especially, Li et al. have developed a deflectometry method that can achieve 1 arcsecond (4.5 μrad) resolution for a single flat mirror [16]. However, much of the information obtained from normal deflectometry is superfluous for an orientation measurement of a segmented mirror. Moreover, unnecessary calculations accumulate numerical errors. These can include fringe print-through from phase calculation/unwrapping [12] and frequency mask effects in reconstructing the surface [14,15]. Therefore, a more informationally efficient solution (acquiring and processing only the essential data) is highly desired for less noisy, highly dynamic, and simultaneous applications.

We present a Simultaneous Multi-segmented mirror Orientation Test System (SMOTS) which parallels the Shack-Hartmann wavefront sensor (SHWS) [17] in a deflectometry technique. SMOTS directly measures the average slope value of a surface within a certain digital aperture. This method provides only the orientation information for several segments simultaneously and efficiently.

In Section 2 we explain the principles of the technique proposed. Section 3 describes numerical simulation results and analysis. The experimental demonstration and test results are presented in Section 4 with concluding remarks in Section 5.

Optics EXPRESS

2. SMOTS theory

When an image is viewed through a mirror, the angle of mirror determines the viewing direction. Furthermore, variation of the mirror tip-tilt angle causes motion of the image. SMOTS is based on this simple yet powerful scheme for orientation measurement. First, a two-dimensionally multiplexed sinusoidal pattern is imaged by a camera [Fig. 1 left]. We take the second picture after tilting the mirror. The updated pattern has a different phase [Fig. 1 right]. The phase shift contains the orientation information of the mirror. Once you measure the distance from the mirror to the pattern, the orientation angle is calculated from the phase shift of the sinusoidal pattern.

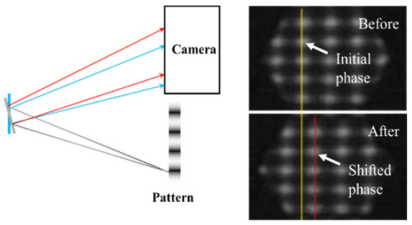

Fig. 1. Schematic SMOTS configuration (left) and the image of two-dimensionally multiplexed sinusoidal pattern captured by camera (right).

The presented SMOTS uses a conventional LCD monitor and CMOS camera. The camera takes images of the screen in reflection from the mirror and calculates phase shift to obtain the mirror orientation change. The scheme is similar to deflectometry, but the actual data acquisition and processing is different. Traditional deflectometry is based on a reverse Hartmann test [12], which calculates the local slope of the surface under test pixel-by-pixel, measuring high spatial frequency surface features, while SMOTS only measures the overall orientation. For instance, SMOTS does not require mapping between the camera and screen pixels. The orientation is efficiently extracted from the captured images in the Fourier domain as explained in Section 2.1.

SMOTS can be understood as a counterpart of SHWS in deflectometry. Comparing the geometry of a SHWS with SMOTS is depicted in Fig. 2. The SHWS was invented by Roland Shack in the early 1970s for astronomical purposes, but it has been adopted by various applications [17]. The smart configuration of SHWS placing a micro-lenslet array at the wavefront plane simplifies the process to sample average wavefront slopes within each micro-lenslet. SMOTS uses a digital aperture (binary mask on the camera image) to sample each segment's surface by placing the detector at (or near) the imaging conjugate plane of the mirror. In the SHWS, the deviation of the focused spot position from the reference position directly indicates the current slope. The shifted pattern phase, in SMOTS, has the same direct relationship to the segment's slope. To make an absolute measurement, an 'absolute reference' and calibration is necessary for both SHWS and SMOTS.

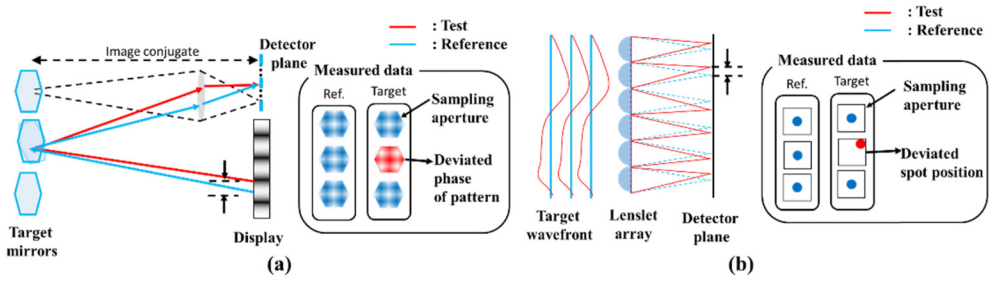

Fig. 2. Comparison between the test methods of the (a) simultaneous multi-segmented mirror orientation test system (SMOTS) and (b) Shack-Hartmann wavefront sensor (SHWS).

Optics EXPRESS

For a SMOTS measurement, we first display the multiplexed sinusoidal pattern on the screen. A camera then captures an image of this pattern through the reflection from the surfaces under test as shown in Fig. 3. Both the surface under test and the screen would be in (or near) focus on the camera detector, which is achieved through a hyperfocal condition. Since the SMOTS camera is a small aperture (e.g., ~1–3 mm diameter) imaging system, such a hyperfocal configuration is available by locating the camera beyond a hyperfocal distance away from the segments under test (for flat segments) or the intermediate image of the sinusoidal pattern (for curved segments). The initial image constitutes the reference sinusoidal pattern, from which a relative orientation measurement is made. When a surface's orientation changes, the sinusoidal pattern captured by the camera shifts linearly with the tip and tilt of the surface. To calculate the change in angle of the surface, we use the difference between first and second image, which is a sheared sinusoidal pattern.

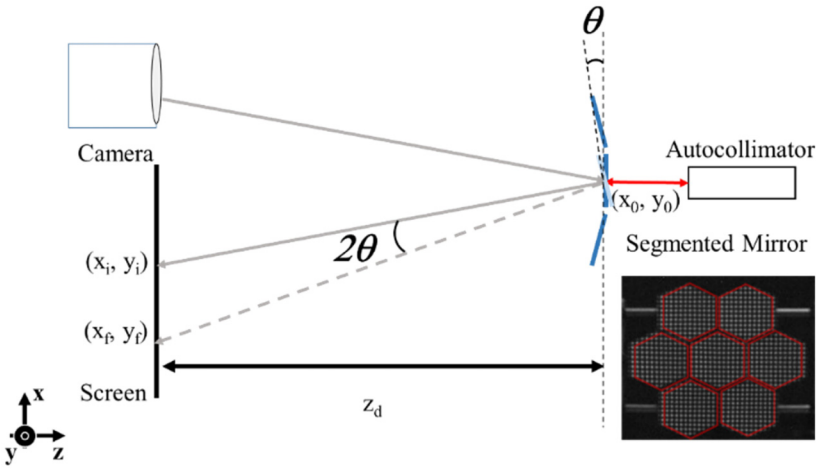

Fig. 3. Experimental SMOTS setup and picture of segmented target mirror used in experiments. The tilt angle θ of a segment causes the sinusoidal pattern to shift.

The data processing pipeline is fundamentally different from the typical deflectometry methods. Deflectometry calculates pixel-by-pixel on the mirror surface to reconstruct the surface shape. However, our method calculates the entire image of the mirror as a single data set and gives the entire mirror tilted angle by using much simpler and quicker Fourier calculation than for surface reconstruction. The two acquired images (before and after) include all the information for every segment, so that we could measure all segmented mirrors simultaneously. In this configuration, any numbers of segments could be measured at one time as long as the camera captures the entire segmented mirror. In addition, due to this benefit, we could obtain relative angle distribution for the segmented mirror in a single implementation.

2.1. Sheared fringe pattern analysis: Fourier analysis

To calculate the change in angle of the surface, a second image is captured by the camera and the first image is subtracted [in Fig. 4(b)]. The different phase in the sinusoidal pattern creates a sheared fringe pattern of the same frequency as the displayed pattern, but with varying amplitude, which directly corresponds to the amount of shift caused by the change in surface orientation as shown in Fig. 4(b). By performing a Fourier analysis on the sheared fringe pattern, we are able to simply and efficiently calculate the amplitude of the sheared fringe pattern. The details are explained below.

Optics EXPRESS

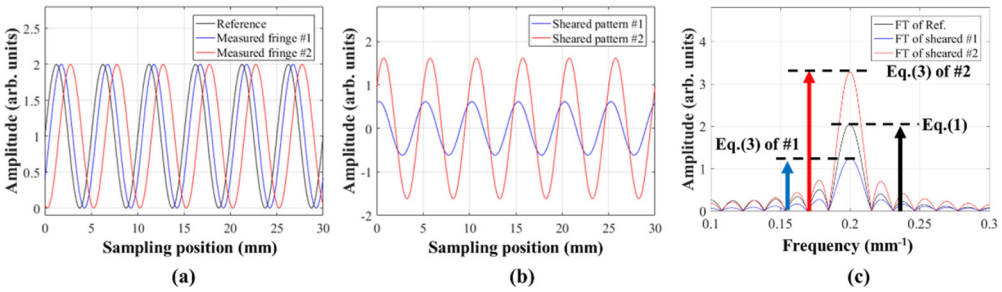

Fig. 4. Fourier analysis steps for sheared pattern calculation.

From the amplitude of the Fourier transform of the sheared sinusoidal pattern, we calculate the amount of phase difference between the reference and the shifted fringe images. The Fourier transform of the difference has the same frequency content as the reference sinusoidal pattern as shown in Fig. 4(c). The ratio of the amplitude in the displayed sinusoidal frequency between the initial [Eq. (1)] and sheared image [Eq. (3)] is converted to the amount of phase shift using Eq. (4). Although a single frequency sinusoidal pattern is displayed on the screen, the camera might capture a distorted pattern due to system aberrations or surface deviations. The frequency of the recorded pattern will be different from the displayed pattern. However, the analysis scheme implemented in SMOTS is insensitive to the additional systematic phase shifts because the reference image will also contain these distortions. Therefore, when the surface angle changes, we are still able to measure the change because it is relative to the reference image. We show a Zemax modeling simulation in Section 3 to verify the phase shift amount for the tilt angle of a variety of mirror shapes. Whatever frequencies are measured by the camera, the shifted phase is calculated by the following equations.

$$\text{Initial pattern frequency bin :} \qquad FT\left(f\left(x\right)\right) = F\left(f\right) \tag{1}$$

$$\text{Shifted pattern frequency bin :} \qquad FT\left(f\left(x+\Delta\right)\right) = e^{-i2\pi\Delta}F(f) \tag{2}$$

$$\text{Sheared pattern frequency bin :} \; FT\left[f\left(x+\Delta\right) - f\left(x\right)\right] = FT\left(f\left(x+\Delta\right)\right) - FT\left(f\left(x\right)\right) = \left(e^{-i2\pi\Delta} - 1\right) F\left(f\right) \tag{3}$$

In order to retrieve the phase information for the sheared pattern in Eq. (3), the shifted phase Δ can be expressed as

$$\Delta = \frac{1}{2\pi} arc\cos\left[1 - \frac{1}{2}\left(\frac{\sqrt{\left[\mathrm{FT}\left(f\left(x+\Delta\right)\right) - \mathrm{FT}\left(f\left(x\right)\right)\right]^2}}{\sqrt{F\left(f\right)^2}}\right)\right] \tag{4}$$

In Eqs. (1)–(4), variable x represents length (on the screen, in our configuration), the transform variable f represents frequency (in m^{-1}), and Δ represents the shifted phase during mirror is moving. The amplitude of the frequency domain of the sheared pattern is simply following a cosine function. We used the imaginary sign of the Fourier transform to resolve sign ambiguity at the cosine function, as shown in Fig. 5. In Fig. 5., Measured #1 and Measured #2 have same phase shift but opposite direction. Due to the same phase shift, the amplitude of FT is same for either case [Fig. 5(b)]. However, the imaginary parts of each case have different sign due to the shifted direction.

Optics EXPRESS

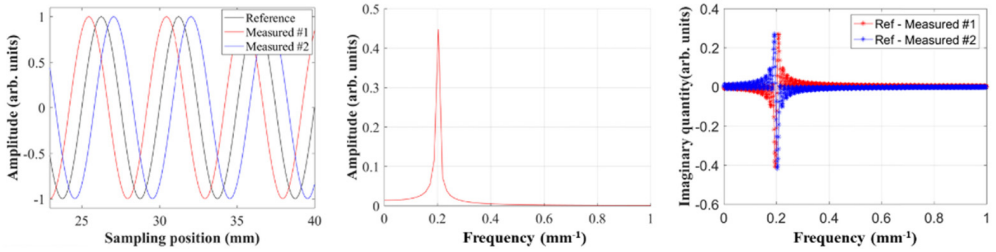

Fig. 5. Sign convention for SMOTS; The FFT amplitude has ambiguity of the shift direction. This direction issue is resolved by using the sign of the imaginary part.

Compared to our shear approach, the standard arctangent phase retrieval using the real and imaginary amplitudes of the Fourier transform can also be considered [18]. If the pattern has a single frequency, then theoretically, this approach will work well. However, if there are mixed frequency contents in the pattern due to imaging distortion or aberrations (discussed in case study 2, Section 3), the phase angle calculation suffers from the finite domain effect with discrete sampling. For instance, if limited by a finite and numerically implemented Fourier transform, a phase shift of a single (or mixed) frequency pattern confined in a limited domain may induce various phase shifts in frequency space as shown in the different y-axis values of the red arrows between Fig. 6(b) and 6(e). However, because of the sheared approach, our method produces correct (i.e., identical) outcome values. It is important to clarify that, for a shifted pattern in the presence of distortion, every sampling point undergoes the same phase shift, not the same distance shift.

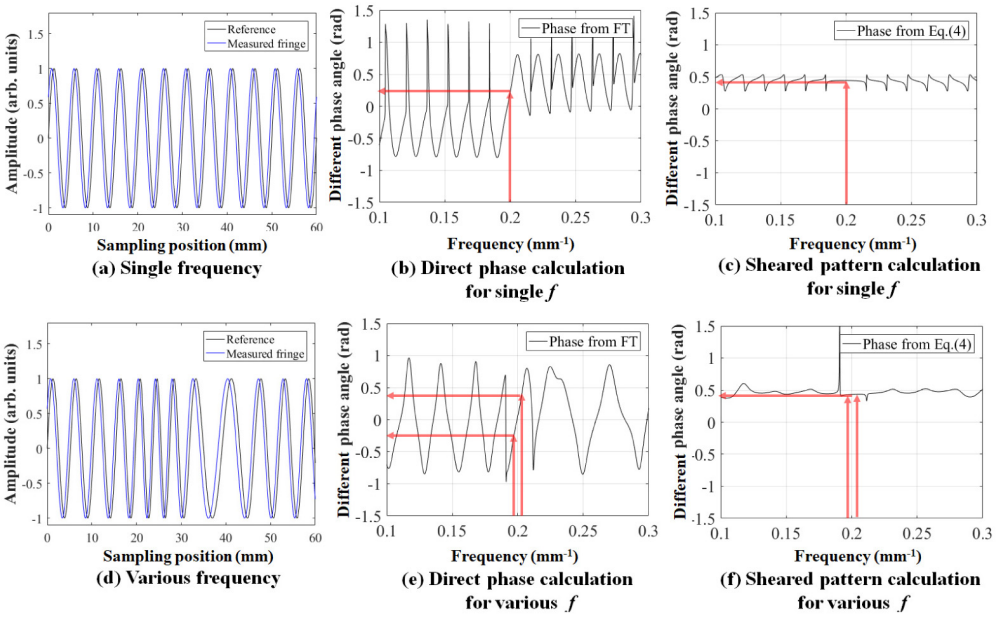

Fig. 6. Comparison between the direct and sheared pattern analysis methods. The same phase shift is applied to (a) single frequency and (b) mixed frequency case. The red arrow shows the nominal frequency of the reference pattern (x-axis) and its calculated phase value (y-axis). (Note: Since the numerical implementation of fast Fourier transform defined in a finite and discrete domain, the phase angle is defined in the entire frequency range. This can be suppressed by applying a threshold outside the expected frequency range, but it is presented without such treatment in this plot. The spikes in the plot represent the 2π jumps in the arctangent calculation.)

Optics EXPRESS

To clarify tilt direction for calculation, we consider the situation in Fig. 3 (tilt angle against to x-axis). Pixel numbers for one period in the display provide the physical length of the phase difference based on the real pixel size under a microscope. The phase Δ in Eq. (3) for the x-axis, gives the position of x_f, defined in Fig. 3 as shown in Eq. (5). The x_i is the initial (i.e., reference) position where the camera looks at the screen.

$$x_f = x_i + \text{Pixel pitch in physical units} \times \text{number of pixels for one period} \times \text{shifted phase}\,(\Delta) \tag{5}$$

The tilt angle θ can be calculated by

$$\theta = \frac{1}{2}\left(arc\tan\left(\frac{(x_i - x_0)}{z_d}\right) - arc\tan\left(\frac{(x_f - x_0)}{z_d}\right)\right) \tag{6}$$

where the z_d is the distance between the mirror and the screen and x_0 is the mirror position along the x-axis.

Although an aberrated pattern imaging by the mirror surface is acquired, this calculation is valid since the 2θ deviation of the ray is still mostly caused by the tilt angle θ within a small angle regime. (See Section 3: Zemax modeling) It is also worth noting that the method response follows a cosine function [Eq. (4)], so the sensitivity of the measurements at both ends of the dynamic range (Δ = 0, 2π) are less than in the middle (Δ = π).

Just like the other sinusoidal pattern-based approaches, there is 2π ambiguity when the tilt angle exceeds a single cycle sinusoidal dynamic range. A long period fringe has a wide dynamic range but loses sensitivity for small angle change. On the other hand, a short period has better sensitivity, but in this case, the phase difference could face 2π ambiguity for a smaller angle change. To resolve this problem, a multiplexing method to include many frequency signals in one picture can be adopted. For instance, a few multiplexed sinusoidal patterns with different periods (not a factor of each other) will reduce such ambiguity as they are clearly distinguishable in the Fourier domain and can be independently processed using the same SMOTS data processing.

3. Zemax numerical case studies for linearity analysis

The SMOTS configuration for a flat mirror application is the most intuitive case. The deflected ray angle is decided by its incidence angle and the surface normal, which relies on the orientation of the mirror. In this way, we can easily understand that a change in the orientation of the flat surface causes a shift of the reflected pattern. However, many mirrors are not flat, and the reflected image of the pattern may be magnified and/or aberrated. To clarify the validity of SMOTS for the various mirror surface shape cases, we present a numerical Zemax modeling analysis [Fig. 7].

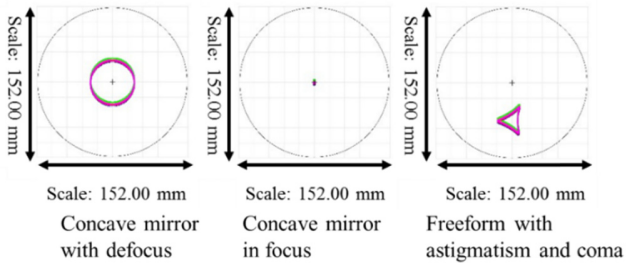

Fig. 7. Reverse-raytracing spot diagram footprints at the screen for the Zemax modeled highly defocused (left), focused (middle), and highly aberrated (right) imaging cases. (Note: Only the outer bounds of the ray distribution are plotted here to distinguish shifted cases.)

Optics EXPRESS

We simulate the point imaging deviation during the mirror tilting. If all the rays reflected from mirrors surface show a slope of two linear angular deviation (calculated by the spot diagram's centroid shift on the screen at a given distance away) with respect to the applied tilt angle, SMOTS can measure tilt angle base on the proportionally deviated pattern. In our reverse-ray tracing simulation, the rays travel from an arbitrary detector plane, which becomes a conjugate plane to the camera detector in a real implementation using a specific camera with lens, to the mirror and reflects back towards the display screen. Various spot diagram footprints showing the extreme extents of simulation cases are shown in Fig. 7.

3.1. Case study 1: Linearity check for defocused imaging case

The SMOTS camera detector plane is focused on the mirror under test in order to apply the digital aperture/mask on each segment as explained in Section 2. Although a hyper-focal condition makes the image of the sinusoidal pattern focused at the same time, there will be always some amount of defocus depends on the specific mirror power reimaging the screen at a certain intermediate image plane. Thus, confirming the pattern shift linearity for a defocused case is critical.

To analyze an extreme defocusing case, for various field points, we used five source points along the x-axis leaving the arbitrary detector plane. A 50 mm diameter mirror with a radius of curvature 500 mm was located 1000 mm away from the detector. Thus, in this case, the intermediate focusing plane (i.e., conjugate plane) is located around 500–250 mm away from the mirror as shown in the schematic diagram in Fig. 8(a). This reverse configuration exactly simulates an extreme defocused case for the sinusoidal pattern finally imaged by a given SMOTS camera (focused on the mirror, not the sinusoidal pattern).

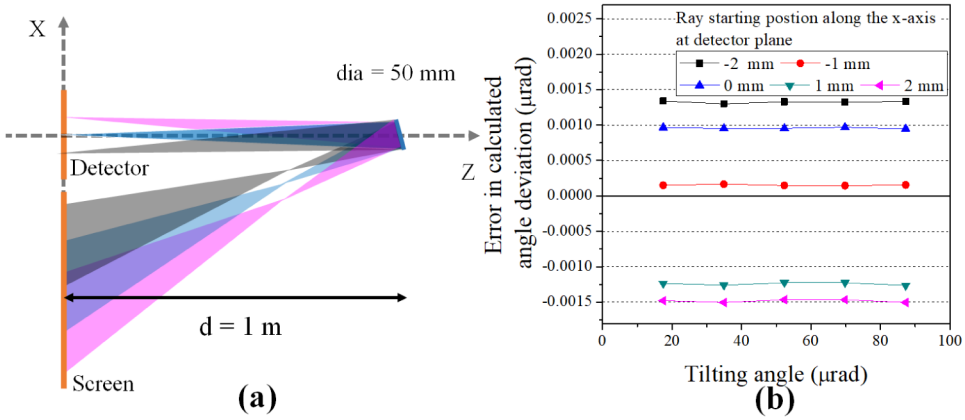

Fig. 8. (a) A schematic reverse Zemax model (showing only three field points) for the linearity check simulating a defocused sinusoidal pattern case. (b) The error in the calculated angle is plotted as a function of input mirror tilting angle for the five field points.

In Fig. 8(b), the errors (i.e., difference) between the simulated tilt angle and the calculated angle from 0 to 90 μrad are presented. In this configuration, the camera captures a slightly distorted picture, and the spot is not now a perfect disk. However, as shown in Fig. 8(b), the deviation from the expected linear angle deviation is well within ± 0.0015 μrad, which is the numerical error range of the simulation. Thus, the defocus effects and off-axis imaging does not affect the linearity of the fringe shifts.

3.2. Case study 2: Linearity check for aberrated imaging case

Certain types of SMOTS configuration and mirror surface shapes (e.g., freeform) might image the sinusoidal pattern with distortions and other aberrations. Unlike the typical deflectometry, the distortion and aberrations should not affect the presented data processing

Optics EXPRESS

accuracy as long as the overall mean phase shift of the pattern is linear. In this case study, a mirror with comatic (Standard Zernike 7th term coefficient: 0.4 mm) and astigmatic (Standard Zernike 5th and 6th term coefficients: −0.3 mm and 0.3 mm) aspheric surface departure was placed at a distance from the screen equal to its radius of curvature (1000 mm) as shown in Fig. 9(a). The errors in the processed angle against the input tilt angle are within ± 0.0015 µrad (similar to case study 1) as shown in Fig. 9(b). This result confirms that the spot position shift at the screen plane is also linear for the aberrated imaging case.

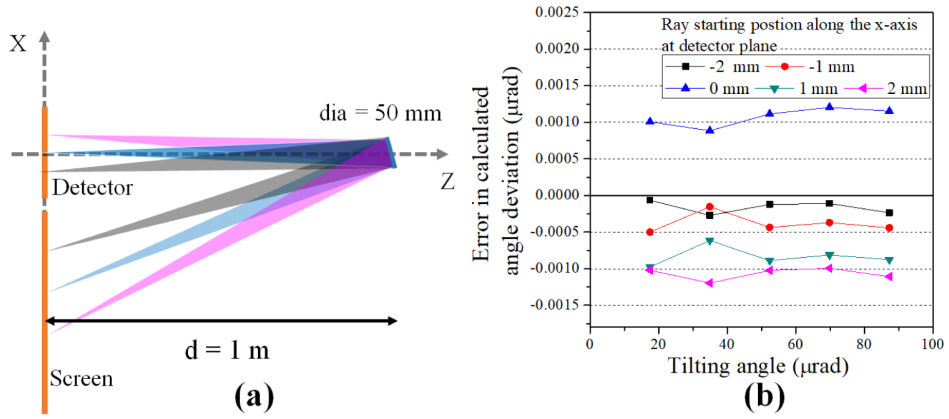

Fig. 9. (a) A schematic reverse Zemax model (showing only three field points) for the linearity check simulating an aberrated sinusoidal pattern case. (b) The error in the calculated angle is plotted as a function of input mirror tilting angle for the five field points.

3.3. Case study 3: Linearity check for multiple segments case

The third case study confirms the linearity for a multiple mirror configuration. We simulated a situation where multiple concave mirror segments are being measured. The segmented concave mirrors have 1000 mm radius of curvature and are placed 1000 mm away from the screen and detector as shown in Fig. 10(a). All three mirrors are concave spherical mirrors and have arbitrary initial tilt angles. The tilt angle of each mirror was changed up to ~90 µrad and the calculated shift angles were compared with the input tilt angles. As shown in Fig. 10(b), the errors are well within 0.002 µrad level for all three segments. All the Zemax modeling results show that SMOTS can measure the angle variation of any mirror and in a segmented situation.

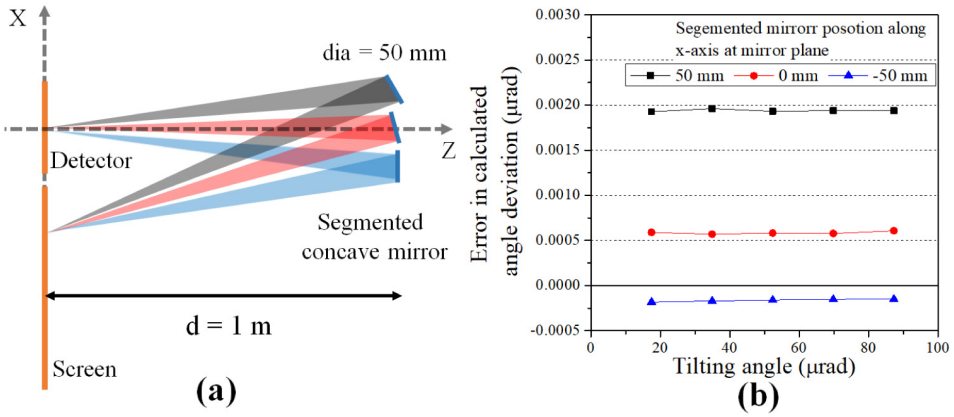

Fig. 10. (a) A schematic reverse Zemax model for the linearity check simulating multiple mirror segments. (b) The error in the calculated angle is plotted as a function of input mirror tilting angle for the three segments.

Optics EXPRESS

4. Experimental demonstration

In order to experimentally validate SMOTS, we used seven hexagonal flat mirror segments to represent a typical arrangement. The center mirror has two Piezoelectric inertia motors (Thorlabs, PIA25) controlling tip and tilt angles to microradian precision. Other mirrors were attached to kinematic mirror mounts (Thorlabs, KM100). An off-the-shelf monitor (Dell, 1097FP) and camera (Pointgrey, FL3-U3-13Y3M-C) were utilized in the setup. We concurrently crosschecked the results with a photoelectric autocollimator (Möller-Wedel, ELCOMAT 3000) as a reference. The overall configuration of the experimental SMOTS setup is shown in Fig. 3.

The two-dimensional sinusoidal pattern was used to measure tip and tilt at the same time. A binary digital mask was applied to the camera detector image on each mirror segment during the image processing such that only the pattern in each masked area was used to calculate the corresponding mirror orientation change.

4.1. SMOTS and autocollimator comparison

The autocollimator oriented a flat mirror, then SMOTS was aligned to see the reflected pattern through the camera. We took an initial picture of the pattern and set this as the reference image because we measure the change in angle from the initial orientation.

We tested SMOTS across its dynamic range, from large angular change steps (~100 μrad) to fine angular change steps (~3 μrad). The distance from the mirror to the screen is 2020 ± 5 mm, and the pixel size of the screen is 294 μm. One period of the two-dimensional sinusoidal pattern was 30 pixels (8.82 mm). While scanning the mirror angle, the measured angle from both SMOTS and autocollimator was recorded concurrently [Fig. 11 and 12].

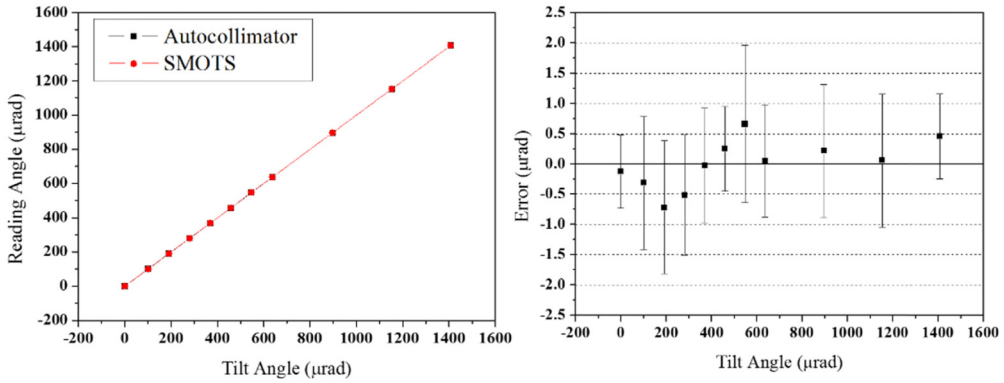

Fig. 11. Large dynamic range with large step size measurement comparison (left) between SMOTS and autocollimator for a flat mirror tilted up to ~1400 μrad. The difference between the two measurements (right) shows less than 0.8 μrad RMS errors. (Note: The error bars represents ± 1 σ standard deviation for 30 data measurements.)

Ten sets of autocollimator data were acquired in 10 s and averaged. Fifty SMOTS data sets were acquired to statistically evaluate the performance. As shown in Figs. 11 and 12, the errors for both ends of the dynamic range are about 0.8 μrad RMS, which is smaller than the noise (error bar) of the data. The noise comes from the CMOS white noise and the blinking of the monitor. The fully random intensity fluctuation (white Gaussian noise over time) of every single pixel can generate frequency errors in the frequency domain. Therefore, even though we chose a specific range of frequency domain in the orientation calculation, we cannot be free from such random noise.

Optics EXPRESS

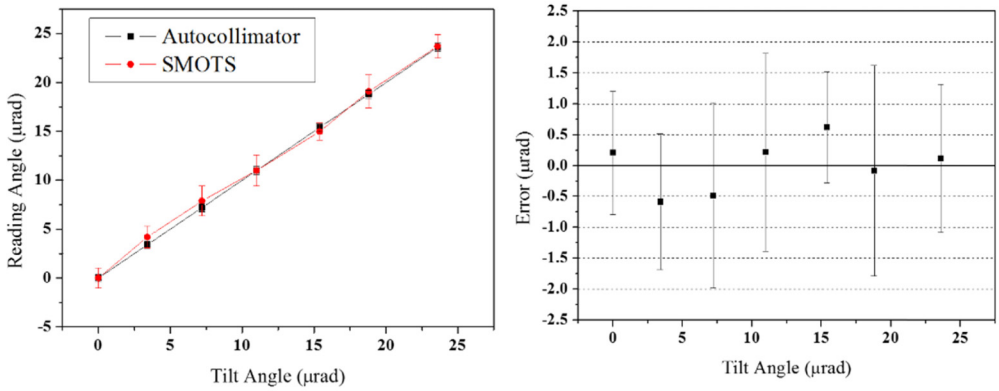

Fig. 12. The small dynamic range with fine step size measurement comparison (left) between SMOTS and autocollimator for a flat mirror tilted up to ~1400 μrad. The difference between the two measurements (right) shows less than 0.8 μrad RMS errors. (Note: The error bars represent ± 1 σ standard deviation for 30 data measurements.)

4.2. Simultaneous multiple mirror segments measurement

Multiple hexagonal mirror segments were tested using the SMOTS to demonstrate its simultaneous capability. In order to highlight its information efficient data processing, a high-speed experiment updating the tip-tilt values at ~15 Hz (with Intel® Xeon® CPU E3 −155M v5, 2.80 GHz) was performed and a snapshot image is shown in Fig. 13. (The most time-consuming process is the image acquisition from the camera detector.)

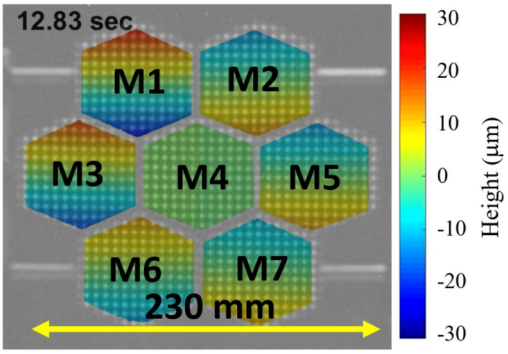

Fig. 13. A snapshot image of the seven hexagonal segments in SMOTS detector showing the over-layered seven digital apertures and calculated instantaneous tip-tilt. The ~15 Hz real-time measurement result is present in Visualization 1.

The simultaneous capability enables real-time compensation such as distinguishing meaningful orientation data from accidental effects such as vibration. As a demonstration, in Fig. 14 (left), a change in tilt angle on M4 was applied at 4 s but an environmental perturbation was introduced around 12 and 15 s duration. By monitoring the entire seven segments together, the environmental incident was successfully recognized as a common motion and compensated (or can be ignored during the data analysis) in the M4 calculation as shown in Fig. 14 (right) and Visualization 2. In a related scenario, any misaligned orientation of SMOTS is distinguished easily because all the mirrors will have the same amount of tip and tilt as a common value. Once the camera grabs the image of the segment, the identical relative angles will be given with a different placement of the setup.

Optics EXPRESS

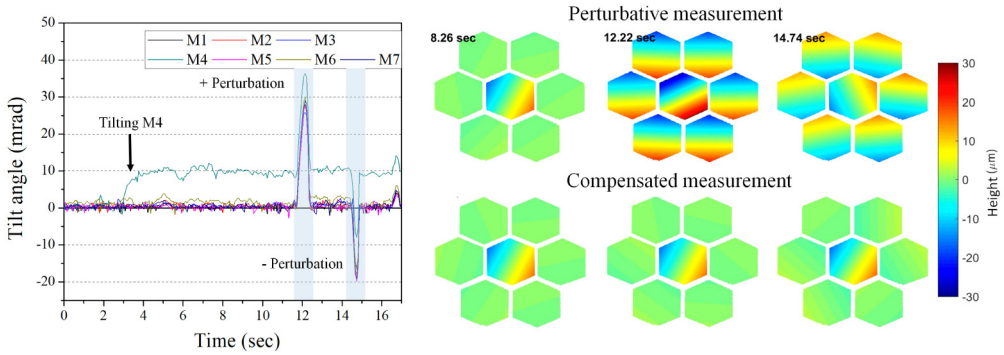

Fig. 14. (left) Simultaneous orientation measurement plot of the seven hexagonal segments using SMOTS. An environmental perturbation was introduced around 12 and 15 s duration. (right) Time sequence snapshots of the seven segments orientation for the perturbed case and the compensated case [Visualization 2].

4.3. Two concave mirror measurement

Two concave mirrors with 200 mm radius of curvature were measured simultaneously using the SMOTS configuration. In order to verify the accuracy, we compared the results using autocollimator data using the same autocollimator as Section 4.1. Since an autocollimator cannot measure two mirrors at the same time, we tested only one of the two mirrors from behind using its flat back surface (depicted in Fig. 3). This highlights the simultaneous measurement capability of SMOTS. The distance from the mirror to the screen was 434 ± 2 mm, and the one period of the two-dimensional sinusoidal pattern was 30 pixels (8.82 mm). It is worth to note that the distance from the mirror to the screen does not have to be same as the mirror's radius of curvature (200 mm) as SMOTS works with hyper-focal condition. While tilting the both mirrors, the measured angle from both instruments was recorded and compared.

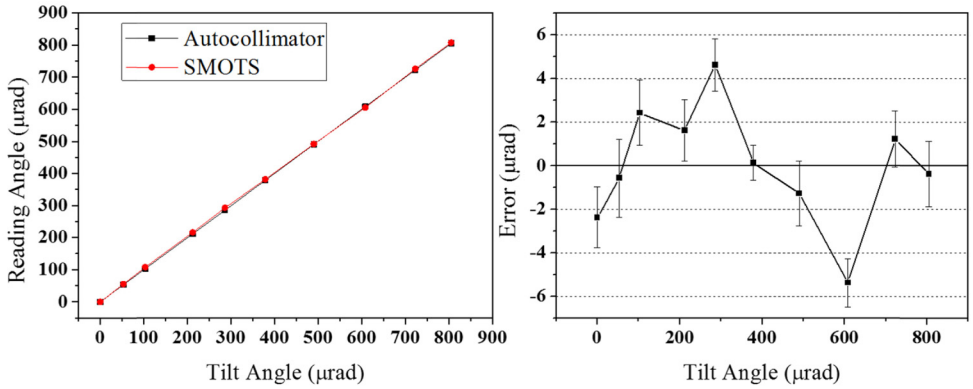

Fig. 15. The tilt measurement comparison (left) and the difference (right) between SMOTS and autocollimator for a concave mirror tilted up to ~800 μrad. (Note: The error bars represents ± 1 σ standard deviation for 30 data measurements.)

In contrast to the flat mirror result [Section 4.1], this result has more standard deviation, as shown in Fig. 15. Unlike the flat mirror tip-tilting, the curved mirror rotation is much more sensitive to its pivot point. In our experimental setup, the rotation axis was not exactly located at the vertex of the mirror surface due to practical limitations of the mounting hardware fixtures. Such a non-ideal rotation in our experimental set up affected our measurement accuracy and degraded the performance to an error level of 2.7 μrad RMS as shown in Fig. 15

Optics EXPRESS

(right). In practice, for a high precision mirror tip-tilt control system, the actuators and/or mounting fixtures are often designed and calibrated to prevent or minimize this effect.

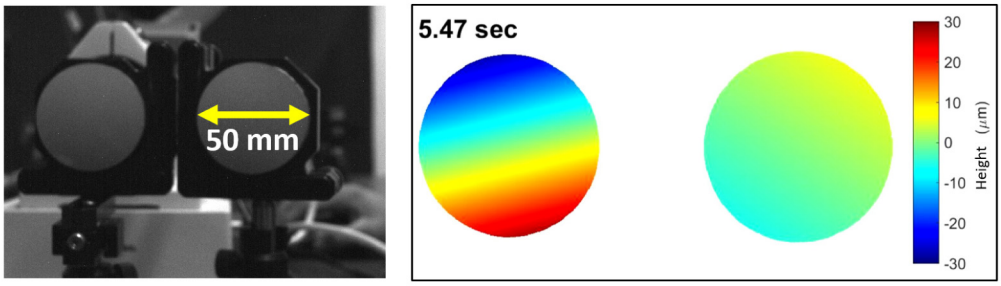

Fig. 16. Picture of the target using two concave mirrors (left) and one frame of measured SMOTS data showing the orientations of the mirrors (right) [Visualization 3].

Similar to the multiple hexagonal segments case, a simultaneous measurement for two pieces of a concave mirror was also performed (Fig. 16 is a snapshot image of Visualization 3). As a side note, due to the smaller number of segments (compared to the seven segments in Section 4.2), the measurement was made and processed at around 23 Hz using the same hardware and software.

5. Conclusion

We developed the Simultaneous Multi-segmented mirror Orientation Test System (SMOTS) with an off-the-shelf camera and display. Without precise calibration, SMOTS can measure angular changes of flat and curved mirrors with an RMS error of 0.8 μrad and 2.7 μrad, respectively. SMOTS measures many segmented mirrors simultaneously as long as the field of view of the camera can cover all the segments and each digital aperture has a sufficient sample of the sinusoidal pattern. Furthermore, due to the simple and robust sheared sinusoidal pattern approach, high-speed implementation (e.g., 15 Hz for seven hexagonal segments) is available for real-time monitoring or compensation.

The accuracy of this method is limited by the resolution of the camera and screen. To make higher precision metrology, we need to display a small period fringe on the screen, and the camera needs to capture the image without aliasing. A longer distance between the mirror and screen can improve the resolution, but a higher resolution camera is required to ensure sufficient sampling. All these limitations are mainly hardware issues, not the fundamental boundaries of the concept or the data processing.

The accuracy and precision of SMOTS is worse than a conventional autocollimator and interferometric method. However, it has a larger dynamic range with a real-time simultaneous capability for multiple mirrors within the camera's field of view and is available to various surface shapes. The relative orientation measurement for multiple segmented mirror system can benefit system level monitoring, vibration compensating, re-adjusting (back to a reference or initial stage), or active controlling in a closed-loop.

Acknowledgment

This research was made possible in part by the Technology Research Initiative Fund (TRIF) Optics/Imaging Program, through the College of Optical Sciences at the University of Arizona, the Post-processing of Freeform Optics project supported by the Korea Basic Science Institute, and the Friends of Tucson Optics (FoTO) Endowed Scholarships in Optical Sciences. The authors would also like to acknowledge the II-VI Foundation Block-Gift Program for helping support general deflectometry research in the LOFT group.